Available online at www.sciencedirect.com
SCIENCE DIRECT®
Journal of Sound and Vibration 273 (2004) 569–583
JOURNAL OF SOUND AND VIBRATION
www.elsevier.com/locate/jsvi

# Effects of hysteretic and aerodynamic damping on supersonic panel flutter of composite plates

Kyo-Nam Koo[a,*], Woo-Seok Hwang[b]

[a] School of Transportation Systems Engineering, University of Ulsan, Ulsan 680-749, South Korea
[b] School of Automotive, Industrial and Mechanical Engineering, Daegu University, Gyeongbuk 712-714, South Korea

Received 20 January 2003; accepted 29 April 2003

**Abstract**

The governing equation for the finite element analysis of the panel flutter of composite plates including structural damping is derived from Hamilton's principle. The first order shear deformable plate theory has been applied to structural modelling so as to obtain the finite element eigenvalue equation. The unsteady aerodynamic load in a supersonic flow is computed by using the linear piston theory. The critical dynamic pressures for composite plates have been calculated to investigate the effects of structural damping on flutter boundaries. The effects are dependent on fiber orientation because flutter mode can be weak or strong in the fiber orientation of composite plates. Structural damping plays an important role in flutter stability with low aerodynamic damping but would not affect the flutter boundary with high aerodynamic damping.


## 1. Introduction

Panel flutter is a dynamic instability of the thin skin of flight vehicles occurring at a critical velocity of the airflow passing over it. Jordan [1] is known as the first person who was aware of panel flutter on flight structures and suggested that a lot of early V-2 rocket failures might have resulted from panel flutter. Many studies [2–8] on the panel flutter of isotropic plates have been carried out since the 1950s. A lot of papers [9–11] attempted the panel flutter analysis of composite plates after composite materials were broadly used in the aerospace structures of the 1980s.

Research on the effect of structural damping on the panel flutter of composite plates, to the authors' knowledge, has not been reported whereas many papers have investigated the effects on

*Corresponding author. Fax: +82-52-259-1681.
*E-mail address:* knkoo@mail.ulsan.ac.kr (K.-N. Koo).

0022-460X/03/$ - see front matter 
doi:10.1016/S0022-460X(03)00514-5

the panel flutter of isotropic plates. In general, damping in composite plates is a favorable property in the aspect of passively controlling dynamic responses. However, the uniformly distributed damping due to structural deformation such as bending may reduce the stability of panel flutter. Ellen [5] illustrated that hysteretic damping $ig(\partial^n w/\partial x^n)$ and viscous damping $ig\omega(\partial^n w/\partial x^n)$ where $g$ is the structural damping coefficient can destabilize the system by making the total amount of damping smaller. It means that the system is stabilized for $n = 0$ but the system can be destabilized for $n > 0$. Lottati [12] showed that viscous damping reduces the stability of the isotropic beam. Though Oyibo [13] analyzed the panel flutter of composite plates, his taking $n = 0$ resulted in a neglect of the uniformly distributed damping due to bending deformation. It can be said that his results did not reflect the correct damping mechanism of composite plates and the effect of fiber orientation.

In this paper, the finite element method formulates the equation of motion for the damped panel flutter of composite plates that is modelled using the first order shear deformable plate theory. High Mach number approximation to the linear potential flow theory, i.e., the linear piston theory that is suitable for $M > \sqrt{2}$ is utilized to compute the unsteady aerodynamic load on the panel. Generally, there is no satisfactory model for damping. This paper adopts the hysteretic damping model since it is more realistic than the viscous damping model in structural vibration. The effect of structural damping on the flutter boundaries of composite plates is investigated in relationship to the change of fiber orientation and the amount of aerodynamic damping.

## 2. Governing equations

The displacement field in the first order shear deformable plate theory can be expressed in the form

$$\begin{Bmatrix} u \\ v \\ w \end{Bmatrix} = \begin{Bmatrix} u_0 \\ v_0 \\ w_0 \end{Bmatrix} - z \begin{Bmatrix} \phi_x \\ \phi_y \\ 0 \end{Bmatrix}, \tag{1}$$

where $u$, $v$, and $w$ are the displacement components in the $x$ , $y$ , $z$ directions, respectively; $\phi_x$ and $\phi_y$ are the rotations about $y$ and $x$ axes, respectively; and the subscript 0 denotes the mid-plane.

Hamilton's principle formulates the finite element equation of damped panel flutter as follows:

$$\int_{t_1}^{t_2} \delta(T - U + W_{nc})\,\mathrm{d}t = 0, \tag{2}$$

where $T$ is the kinetic energy, $U$ is the potential energy, $W_{nc}$ is the work done by non-conservative forces, and $\delta$ is a variational operator.

The kinetic energy for symmetric laminated plate can be obtained:

$$\int_{t_1}^{t_2} \delta T\,\mathrm{d}t = \int_{t_1}^{t_2} \int_V \rho \dot{\mathbf{u}}^{\mathrm{T}} \delta \dot{\mathbf{u}}\,\mathrm{d}V\,\mathrm{d}t = -\hat{m} \int_{t_1}^{t_2} \int_0^a \int_0^b (I\ddot{\phi}_x \delta\phi_x + I\ddot{\phi}_y \delta\phi_y + \ddot{w}\delta w)\,\mathrm{d}x\,\mathrm{d}y\,\mathrm{d}t, \tag{3}$$

where $\rho$ is the density of plate, $\mathbf{u}^{\mathrm{T}} = \{u\ v\ w\}$, $\hat{m} = \rho h$ and $I = (\int_{-h/2}^{h/2} \rho z^2\,\mathrm{d}z)/\rho h$. The bending strain energy for symmetric laminated plate is given by

$$\int_{t_1}^{t_2} \delta U\,\mathrm{d}t = \int_{t_1}^{t_2} \int_V \boldsymbol{\sigma}^{\mathrm{T}}\delta\boldsymbol{\varepsilon}\,\mathrm{d}V\,\mathrm{d}t = \int_{t_1}^{t_2} \int_0^a \int_0^b \boldsymbol{\chi}^{\mathrm{T}}\mathbf{D}\delta\boldsymbol{\chi}\,\mathrm{d}x\,\mathrm{d}y\,\mathrm{d}t. \tag{4}$$

Here

$$\boldsymbol{\chi}^{\mathrm{T}} = \left\{ \left(\frac{\partial\phi_x}{\partial x}\right) \left(\frac{\partial\phi_y}{\partial y}\right) \left(\frac{\partial\phi_x}{\partial y} + \frac{\partial\phi_y}{\partial x}\right) \left(\frac{\partial w}{\partial y} + \phi_y\right) \left(\frac{\partial w}{\partial x} + \phi_x\right) \right\}$$

and $\mathbf{D}$ is the bending stiffness of laminated plates and defined as

$$D_{ij} = \int_{-h/2}^{h/2} (\bar{Q}_{ij})_k z^2\,\mathrm{d}z \quad \text{for } i,j = 1,2,3,$$

$$D_{ij} = \int_{-h/2}^{h/2} (\bar{Q}_{ij})_k\,\mathrm{d}z \quad \text{for } i,j = 4,5, \tag{5}$$

where $\bar{\mathbf{Q}}_k = \mathbf{R}_k^{-1}\mathbf{Q}\mathbf{R}_k^{-\mathrm{T}}$ is the transformed reduced stiffness of the $k$th layer; $\mathbf{R}_k^{-1}$ is the inverse of the transformation matrix $\mathbf{R}_k$ and $\mathbf{R}_k^{-\mathrm{T}}$ is the transpose matrix of $\mathbf{R}_k^{-1}$; $\mathbf{Q}$ is the reduced stiffness matrix of an orthotropic lamina; and the definitions of $\mathbf{R}_k$ and $\mathbf{Q}$ can be found in Ref. [14].

The virtual work by non-conservative force $\delta W_{nc}$ is composed of the virtual work by aerodynamic force, $\delta W_A$ and the virtual work by structural damping, $\delta W_D$.

$$\delta W_{nc} = \delta W_A + \delta W_D. \tag{6}$$

Using a first order high Mach number approximation to the linear potential flow theory, which is suitable for $M > \sqrt{2}$, $\delta W_A$ becomes

$$\int_{t_1}^{t_2} \delta W_A\,\mathrm{d}t = \int_{t_1}^{t_2} \int_0^a \int_0^b q\delta w\,\mathrm{d}x\,\mathrm{d}y\,\mathrm{d}t = -\int_{t_1}^{t_2} \int_0^a \int_0^b \left(\beta\frac{\partial w}{\partial x} + \mu\frac{\partial w}{\partial t}\right)\delta w\,\mathrm{d}x\,\mathrm{d}y\,\mathrm{d}t, \tag{7}$$

where $\beta = \rho_a V^2/\sqrt{M^2-1}$, $\mu = \rho_a V(M^2-2)/(M^2-1)^{1.5}$; $\rho_a$, $V$, and $M$ are the density, velocity, and Mach number of free stream, respectively.

Assuming the structural damping to be hysteretic can make $\delta W_D$ expressed by

$$\int_{t_1}^{t_2} \delta W_D\,\mathrm{d}t = -\frac{1}{\omega}\int_{t_1}^{t_2} \int_V \dot{\boldsymbol{\sigma}}^{\mathrm{T}}\bar{\mathbf{H}}\delta\boldsymbol{\varepsilon}\,\mathrm{d}V\,\mathrm{d}t = -\frac{1}{\omega}\int_{t_1}^{t_2} \int_0^a \int_0^b \dot{\boldsymbol{\chi}}^{\mathrm{T}}\mathbf{G}\delta\boldsymbol{\chi}\,\mathrm{d}x\,\mathrm{d}y\,\mathrm{d}t. \tag{8}$$

Here $\bar{\mathbf{H}}$ is a diagonal matrix with non-zero components $\bar{h}_{11} = \eta_x$, $\bar{h}_{22} = \eta_y$, $\bar{h}_{33} = \eta_{xy}$, $\bar{h}_{44} = \eta_{yz}$, $\bar{h}_{55} = \eta_{xz}$ and $\mathbf{G}$ is the damping matrix due to bending and defined as

$$G_{ij} = \int_{-h/2}^{h/2} \bar{Q}_{ij}^H z^2\,\mathrm{d}z \quad \text{for } i,j = 1,2,3,$$

$$G_{ij} = \int_{-h/2}^{h/2} \bar{Q}_{ij}^H\,\mathrm{d}z \quad \text{for } i,j = 4,5, \tag{9}$$

where $\bar{\mathbf{Q}}_k^H = \mathbf{R}_k^{-1}\mathbf{H}\mathbf{Q}\mathbf{R}_k^{-\mathrm{T}}$ and $\mathbf{H}$ is a diagonal matrix with non-zero components $h_{11} = \eta_1$, $h_{22} = \eta_2$ , $h_{33} = \eta_{12}$, $h_{44} = \eta_{23}$, $h_{55} = \eta_{13}$. $\eta_1$ and $\eta_2$ denote the loss factors in $0^\circ$ and $90^\circ$ directions of a lamina, and $\eta_{12}$, $\eta_{23}$, and $\eta_{13}$ are the loss factors by shear.

Substitution of the expressions in Eqs. (3), (4), (7), and (8) into Eq. (2) derives a variational formulation of the problem. The finite element method interpolates the displacements in a linear combination of shape functions like

$$(w, \phi_x, \phi_y) = \sum_{i=1}^{n} (\bar{w}_i, \bar{\phi}_{xi}, \bar{\phi}_{yi}) N_i(x, y), \tag{10}$$

where $N_i(x, y)$ is the Lagrange family of interpolation functions and $n$ is the number of nodes per element.

The finite element equation can be written substituting Eq. (10) into the variational formulation:

$$\hat{m}\mathbf{M}\ddot{\mathbf{u}} + \left(\frac{1}{\omega}\mathbf{C} + \mu\mathbf{M}\right)\dot{\mathbf{u}} + (\beta\mathbf{A} + \mathbf{K})\mathbf{u} = \mathbf{0}. \tag{11}$$

Assuming the vibration to be stationary, i.e., $\mathbf{u}(t) = \bar{\mathbf{u}}e^{i\omega t}$, transforms the flutter equation into the eigenvalue equation:

$$(i\mathbf{C} + \mathbf{K} + \beta\mathbf{A} - \lambda\mathbf{M})\bar{\mathbf{u}} = \mathbf{0}, \tag{12}$$

where an eigenvalue is defined as $\lambda = \omega^2\hat{m} - i\omega\mu$. In the case for $\beta = 0$, composite plate undergoes a damped free vibration with $\mathbf{C}$ and an undamped free vibration without $\mathbf{C}$. If the aerodynamic damping $\mu$ is considered, it is the critical dynamic pressure $\beta_{cr}$ at which the computed aerodynamic damping $\mu = \lambda_I/\sqrt{\lambda_R/\hat{m}}$ coincides with the aerodynamic damping assumed according to the flight condition.

## 3. Numerical results

A nine-noded isoparametric element is employed and only the clamped square plate with the length-to-thickness ratio of $a/h = b/h = 200$ is considered in this paper. Fig. 1 shows the geometric definition of composite plate in airflow.

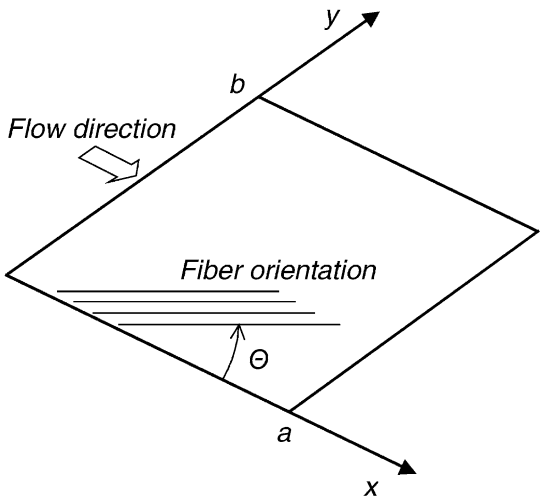


Fig. 1. Geometric definition of composite plates in airflow.

Table 1
Non-dimensional frequencies and flutter bounds for $[0/90_2]_S$ boron/epoxy[a] clamped square plate

| Solution | Non-dimensional frequency, $\sqrt{\lambda_R^*}$ | | | | | | Flutter bounds | |
|---|---|---|---|---|---|---|---|---|
| | 1 | 2 | 3 | 4 | 5 | 6 | $\sqrt{\lambda_R^*}$ | $\beta_{cr}^*$ |
| *Present* | | | | | | | | |
| $6 \times 6$ nine-noded elements | 23.33 | 41.83 | 54.17 | 65.54 | 75.77 | 92.39 | 46.42 | 459.91 |
| *Srinivasan and Babu* [8] | | | | | | | | |
| Integral equation method | 23.33 | 42.36 | 53.77 | 65.56 | 76.52 | 92.76 | 46.09 | 446.36 |
| Series solution | 23.63 | 42.28 | 53.76 | 65.42 | 75.89 | 92.19 | 47.19 | 474.60 |

[a] $E_1 = 213.7$ GPa, $E_2 = 18.6$ GPa, $G_{12} = G_{13} = 5.17$ GPa, $G_{23} = 6.21$ GPa, $v_{12} = 0.28$, $\rho = 2052$ kg/m$^3$.

The non-dimensional natural frequency $\sqrt{\lambda_R^*} = \sqrt{\lambda_R a^4/E_2h^3}$ and non-dimensional critical dynamic pressure $\beta_{cr}^* = \beta_{cr}a^3/E_2h^3$ for a boron/epoxy clamped square plate with $[0/90_2]_S$ are given in Table 1 to show the accuracy of the present analysis. Since both the frequency parameter and the flutter bounds with $6 \times 6$ elements are in a good agreement with the results of Srinivasan and Babu [8], all the plates in this analysis are divided into $6 \times 6$ finite elements.

The composite material used in the analysis is HMS/DX-210 of which properties are given as [15]

$$E_1 = 172.7 \text{ GPa}, \ E_2 = 7.2 \text{ GPa}, \ G_{12} = 3.76 \text{ GPa}, \ v_{12} = 0.3, \ \rho = 1550 \text{ kg/m}^3,$$
$$\eta_1 = 7.162 \times 10^{-4}, \quad \eta_2 = 6.716 \times 10^{-3}, \quad \eta_{12} = \eta_{23} = \eta_{13} = 1.122 \times 10^{-2}. \tag{13}$$

### 3.1. Quasi-isotropic composite plate

Fig. 2 shows the non-dimensional real eigenvalue $\lambda_R^* = \lambda_R a^4/E_2h^3$ and imaginary one $\lambda_I^* = \lambda_I a^4/E_2h^3$ of the critical modes vs. the non-dimensional dynamic pressure $\beta^*$ for a quasi-isotropic plate $[0/\pm 45/90]_S$. The solid line (——) means the eigenvalues when the structural damping $\eta_{ij}$ is neglected, i.e., $\eta_{ij} = 0$; the dashed line (- - - - - -) denotes the eigenvalues when the structural damping $\eta_{ij}$ given in Eq. (13) is included; the centered line (–·–·–) is obtained by increasing the structural damping $\eta_{ij}$ in Eq. (13) by 10 times, i.e., $10 \times \eta_{ij}$. In the case for $\eta_{ij} = 0$, two real eigenvalues $\lambda_R^*$ approach to each other with increasing $\beta^*$ and then merge into a pair of complex conjugate after the flutter occurs. This phenomenon is called frequency coalescence. In the case for $\eta_{ij} \neq 0$, the eigenvalues $\lambda^*$ are complex for any value of $\beta^*$ except for zero. The real parts of two eigenvalues, $\lambda_R^*$ approach to each other but do not coalesce. In this case, flutter occurs when an imaginary part of an eigenvalue $\lambda_I^*$ changes from positive to negative. It is seen that the critical dynamic pressure in the case for $\eta_{ij} \neq 0$ is greatly reduced as compared to that for $\eta_{ij} = 0$. It is observed in Fig. 2 that critical flutter occurs with relation to modes 9 and 10 for both $\eta_{ij} = 0$ and $\eta_{ij}$, but to mode 1 and 2 for $10 \times \eta_{ij}$. It is noted that the flutter in relation to modes 9 and 10, which will be designated the flutter of mode 9/10 hereafter, is a weak flutter instability which becomes

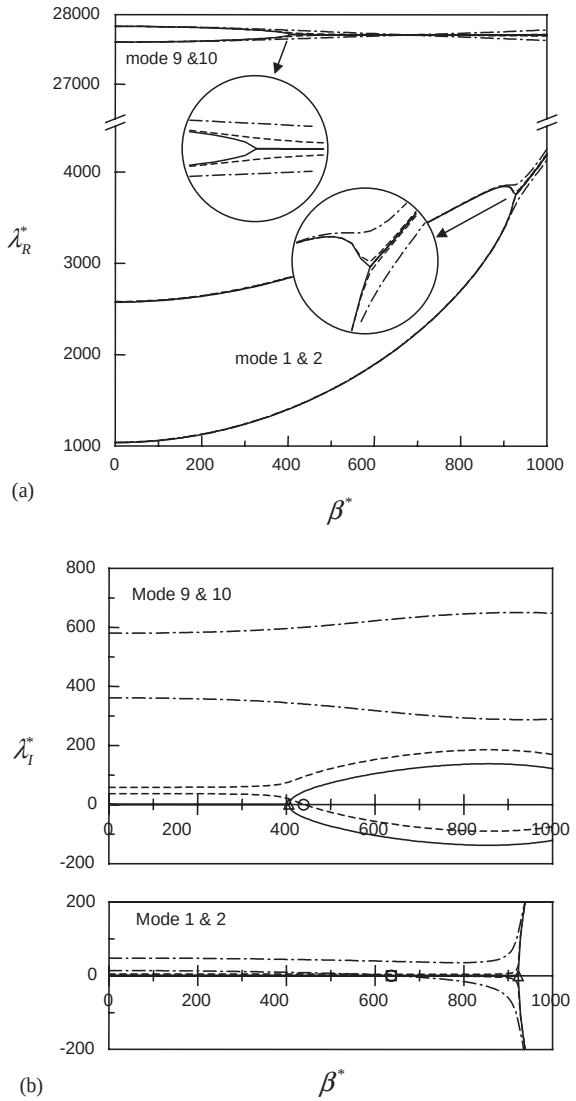


Fig. 2. (a) Real eigenvalue $\lambda_R^*$ and (b) imaginary eigenvalue $\lambda_I^*$ of $[0/\pm 45/90]_S$ clamped square plate. ——, $\eta_{ij} = 0$; - - - - - -, $\eta_{ij}$; – · – · –, $10 \times \eta_{ij}$; △, ○, □, flutter points.

stable with increments of structural damping. The natural mode shapes and flutter mode shapes are illustrated in Fig. 3. It is shown that the flutter mode shapes look like a combination of two related natural modes.

Fig. 4 shows the critical dynamic pressure $\beta_{cr}^*$ versus the magnification factor $n$ of the material loss factors $\eta_{ij}$ of HMS/DX-210 for the flutter of mode 1/2. Neglecting the aerodynamic damping $\mu$, $\beta_{cr}^*$ decreases suddenly and then keeps constant as the loss factor increases. However, the effect of aerodynamic damping makes the critical dynamic pressure decrease gradually as the loss factor increases. The critical dynamic pressures $\beta_{cr}^*$ for the flutter of mode 1/2 in Fig. 5

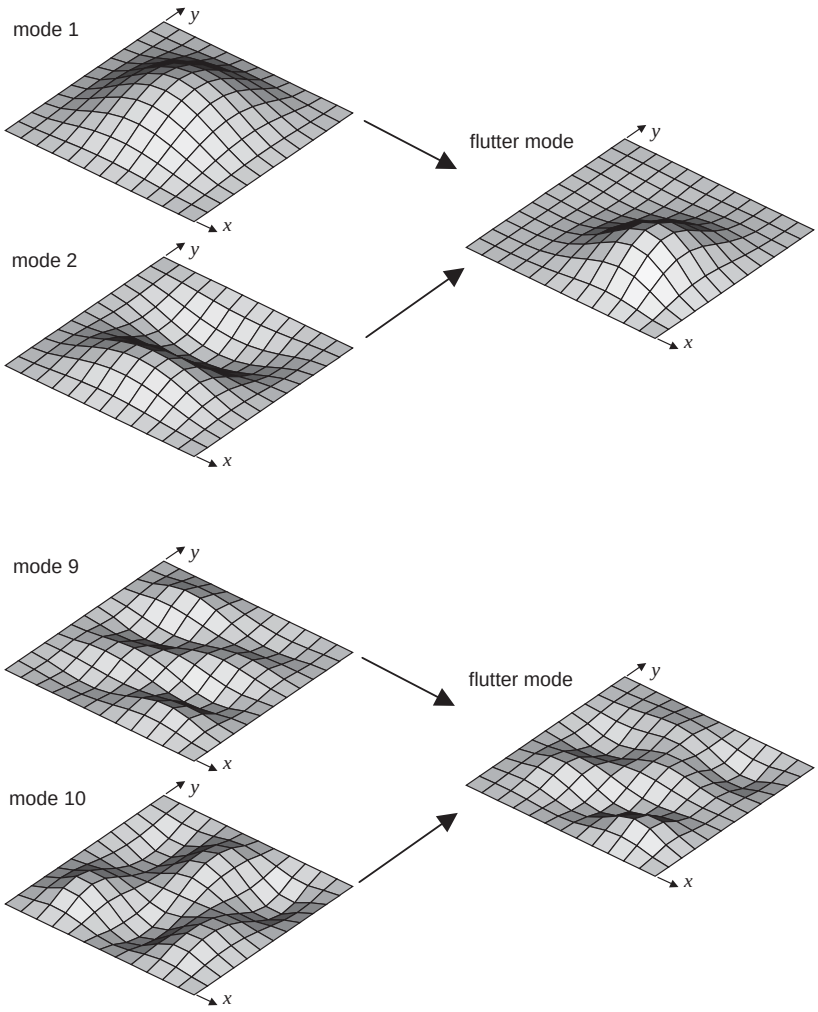


Fig. 3. Natural mode shapes and flutter mode shapes of $[0/\pm 45/90]_S$ clamped square plate.

increases regardless of the magnitude of structural damping as the aerodynamic damping $\mu$ increases.

Fig. 6 illustrates the lowest critical dynamic pressures $\beta^*_{cr}$ versus the magnification factor $n$ of material loss factors $\eta_{ij}$ for several values of $\mu$. It is interesting that instability occurs in the flutter of mode 9/10 when the structural damping is small but in the flutter of mode 1/2 when the structural damping is large. Also, it is worthwhile noting that structural damping may stabilize or destabilize the flutter instability depending on the type of flutter. The flutter of mode 1/2 is destabilized with an increase of the structural damping and the flutter of mode 9/10 which is a weak flutter is stabilized with increase of the structural damping. In comparison with the results in Fig. 5, the lowest $\beta^*_{cr}$ versus $\mu$ for various structural damping shown in Fig. 7 indicates that the effect of aerodynamic damping on the stability of the flutter of mode 9/10 is different from that

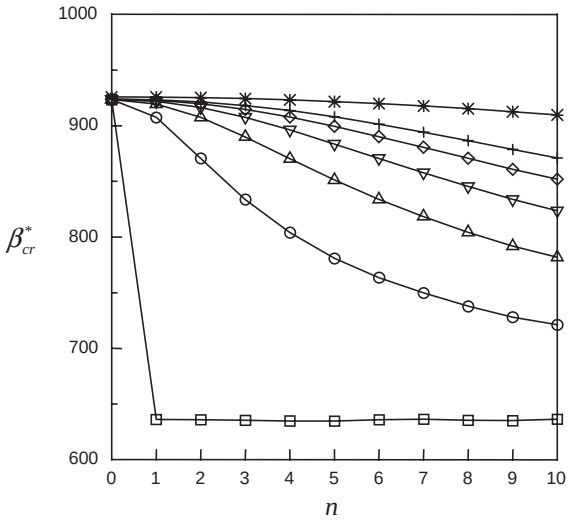


Fig. 4. Effects of structural damping magnitude on critical dynamic pressure of flutter of mode 1/2 for $[0/\pm 45/90]_S$. $\square$, $\mu = 0$; $\bigcirc$, $\mu = 10$; $\triangle$, $\mu = 20$; $\nabla$, $\mu = 30$; $+$, $\mu = 50$; $*$, $\mu = 100$.

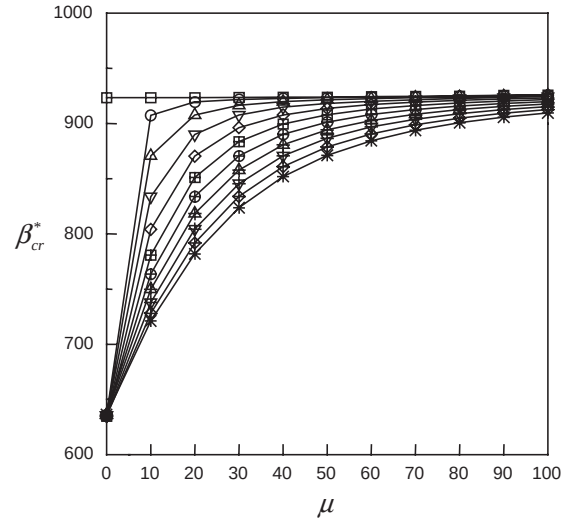


Fig. 5. Effects of aerodynamic damping on critical dynamic pressure of flutter of mode 1/2 for $[0/\pm 45/90]_S$. $\square$, $n = 0$; $\bigcirc$, $n = 1$; $\triangle$, $n = 2$; $\nabla$, $n = 3$; $\diamond$, $n = 4$; $\square$, $n = 5$; $\oplus$ $n = 6$; $\triangle$, $n = 7$; $\nabla$, $n = 8$; $\diamond$, $n = 9$; $*$, $n = 10$.

for the flutter of mode 1/2. The flutter of mode 9/10 shows a nearly constant stability at the large values of aerodynamic damping whereas the flutter of mode 1/2 shows a high increasing rate of stability at the low values of aerodynamic damping.

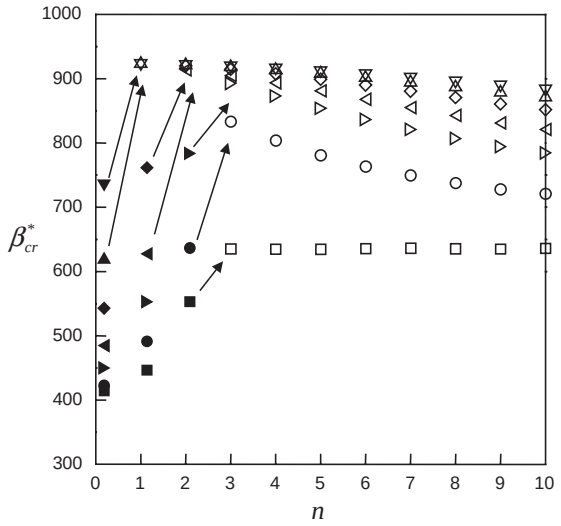


Fig. 6. Lowest critical dynamic pressure for $[0/\pm 45/90]_S$ with variation of structural damping. □, mode 1/2; ▩, mode 9/10 for $\mu = 0$. ○, mode 1/2; ●, mode 9/10 for $\mu = 10$. ▷, mode 1/2; ▶, mode 9/10 for $\mu = 20$. ◁, mode 1/2; ◀, mode 9/10 for $\mu = 30$. ◇, mode 1/2; ◆, mode 9/10 for $\mu = 40$. △, mode 1/2; ▲, mode 9/10 for $\mu = 50$. ▽, mode 1/2; ▼, mode 9/10 for $\mu = 60$.

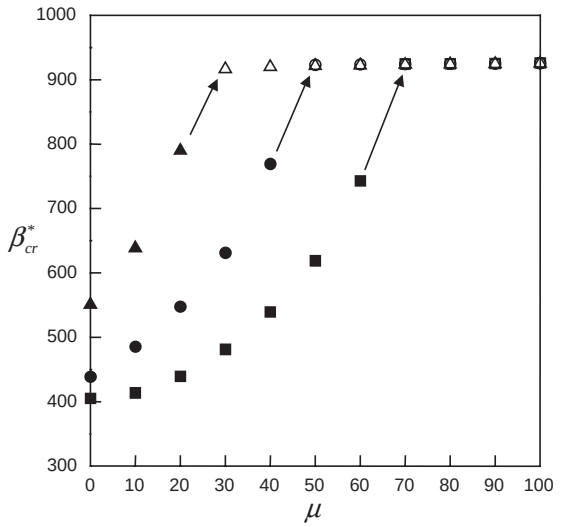


Fig. 7. Lowest critical dynamic pressure of flutter for $[0/\pm 45/90]_S$ with variation of aerodynamic damping. □, mode 1/2; ▩, mode 9/10 for $n = 0$. ○, mode 1/2; ●, mode 9/10 for $n = 1$. △, mode 1/2; ▲, mode 9/10 for $n = 2$.

### 3.2. Orthotropic composite plate

Fig. 8 shows the effects of structural damping on the critical dynamic pressure of $[\theta]_S$ plate with a variation of fiber orientation $\theta$ for three values of aerodynamic damping, $\mu = 0,\ 10,\ 100$. The

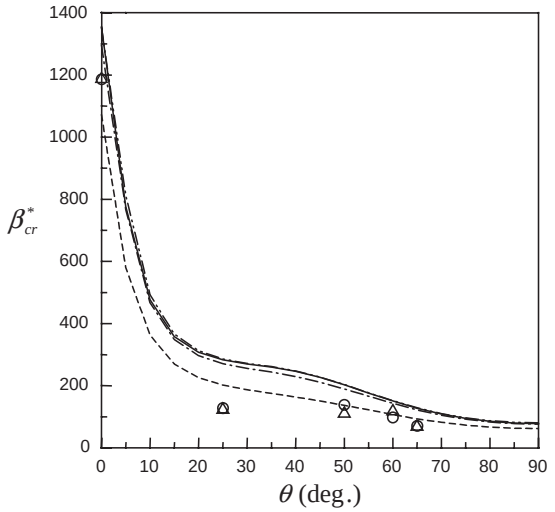


Fig. 8. Critical dynamic pressure versus fiber orientation $\theta$. ——: $\eta_{ij} = 0$, $\mu = 0$; - - - - - -: $\eta_{ij} \neq 0$, $\mu = 0$; – · – · –: $\eta_{ij} \neq 0$, $\mu = 10$; – – – – – – –: $\eta_{ij} \neq 0$, $\mu = 100$; ○: $\eta_{ij} \neq 0$, $\mu = 0$; (△) $\eta_{ij} = 0$, $\mu = 0$.

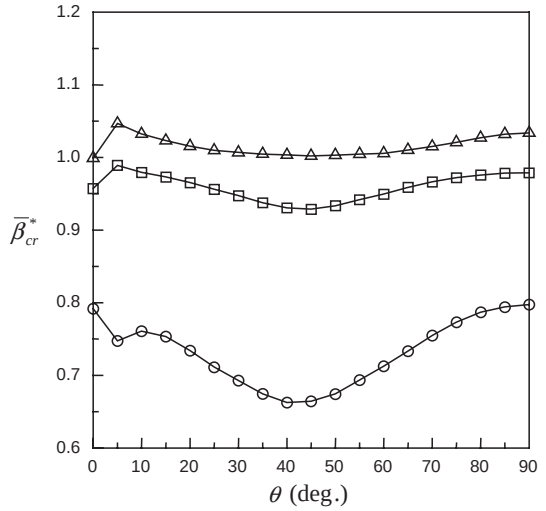


Fig. 9. Ratio of critical dynamic pressure with structural damping to critical dynamic pressure without structural and aerodynamic damping. ○, $\mu = 0$; □, $\mu = 10$; △, $\mu = 100$.

lines in Fig. 8 denote the critical dynamic pressures of the flutter of mode 1/2 except for $\theta = 0°$. where the instability occurs in the flutter of mode 1/6. The symbols circle (○) and triangle (△) mean the critical pressures of flutter modes other than mode 1/2. The critical dynamic pressure decreases as the fiber orientation increases because the bending stiffness in the flow direction, $D_{11}$ decreases with increasing fiber orientation. The critical dynamic pressures of the flutter of mode 1/2 with the structural damping (designated as ——) are much smaller than those without the

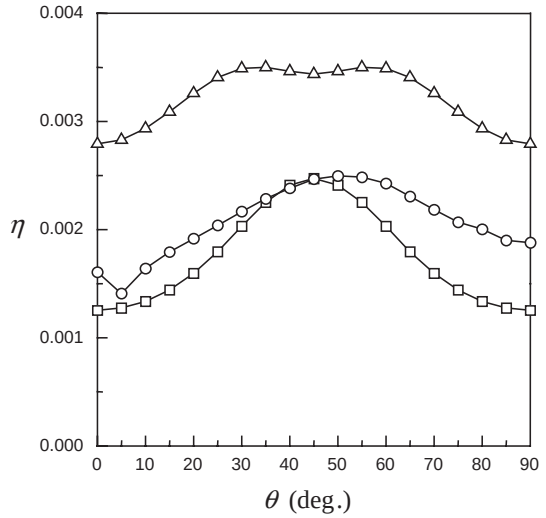


Fig. 10. Modal loss factors versus fiber orientation $\theta$ of first, second and flutter modes. □, first mode; △, second mode; ○, flutter mode.

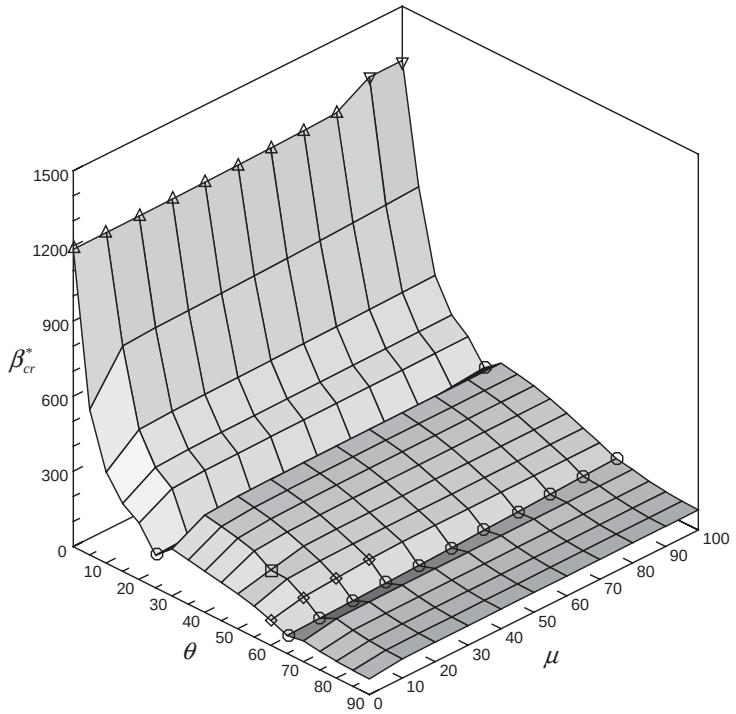


Fig. 11. Lowest critical dynamic pressures of $[\theta]_S$ plate with $\eta_{ij} \cdot$ △, mode 4/6; ▽, mode 1/6; ○, mode 7/8; □, mode 8/9; ◇, mode 9/10.

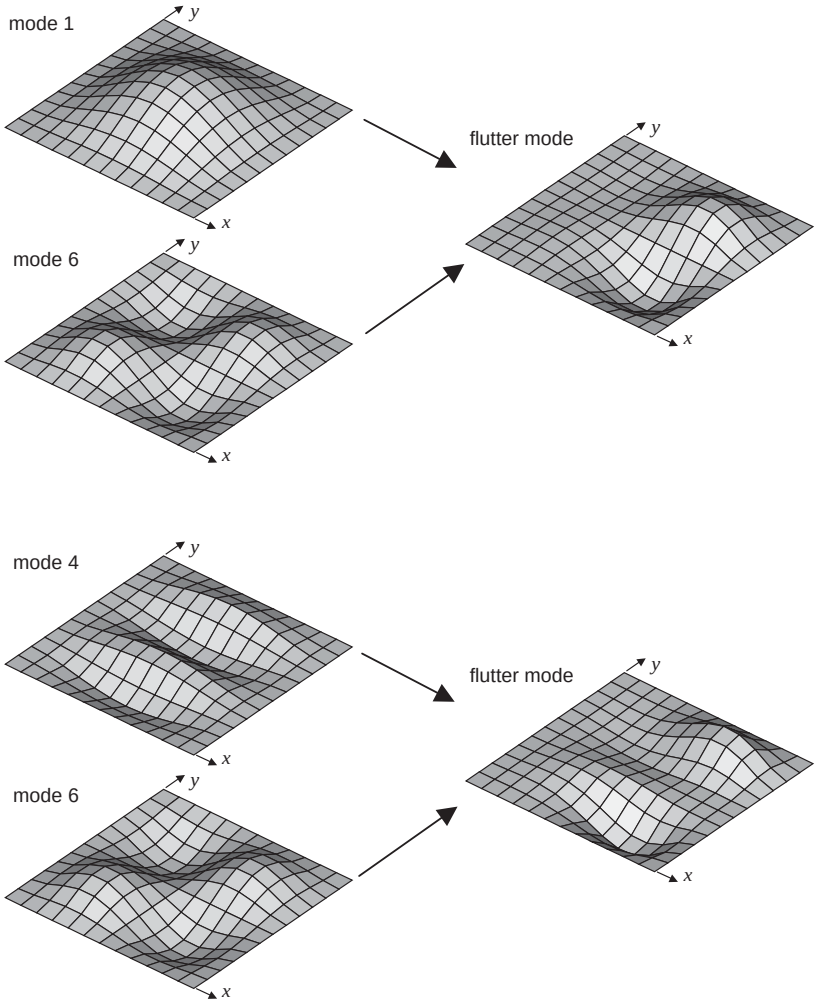


Fig. 12. Natural and flutter mode shapes of $[0]_S$ plate.

structural damping (designated as - - - - - -) and the trends of those two cases are similar to each other. The critical dynamic pressures using the structural damping approach to those without the structural damping for $\mu = 0$ as the aerodynamic damping $\mu$ increases. This is because aerodynamic damping becomes much bigger compared to structural damping. Flutter instability occurs in different modes at some fiber orientations. For example, instability occurs in the flutter of mode 8/9 at $\theta = 50^\circ$, which is weak and structural damping stabilizes the flutter.

The amount of decrement in $\beta^*_{cr}$ by the structural damping in flutter analysis for $\mu = 0,\ 10,\ 100$ is shown in Fig. 9 with a variation of fiber orientation. The instability in Fig. 9 is the flutter of mode 1/2 besides $\theta = 0^\circ$ as is in Fig. 8. $\bar{\beta}^*_{cr}$ denotes the critical dynamic pressures normalized by the dynamic pressure at $\theta = 0^\circ$ when $\eta_{ij} = 0$ and $\mu = 0$. It is observed that a reduction of $\bar{\beta}^*_{cr}$ by structural damping is largest near $\theta = 45^\circ$. The modal loss factors of the natural modes 1, 2 and

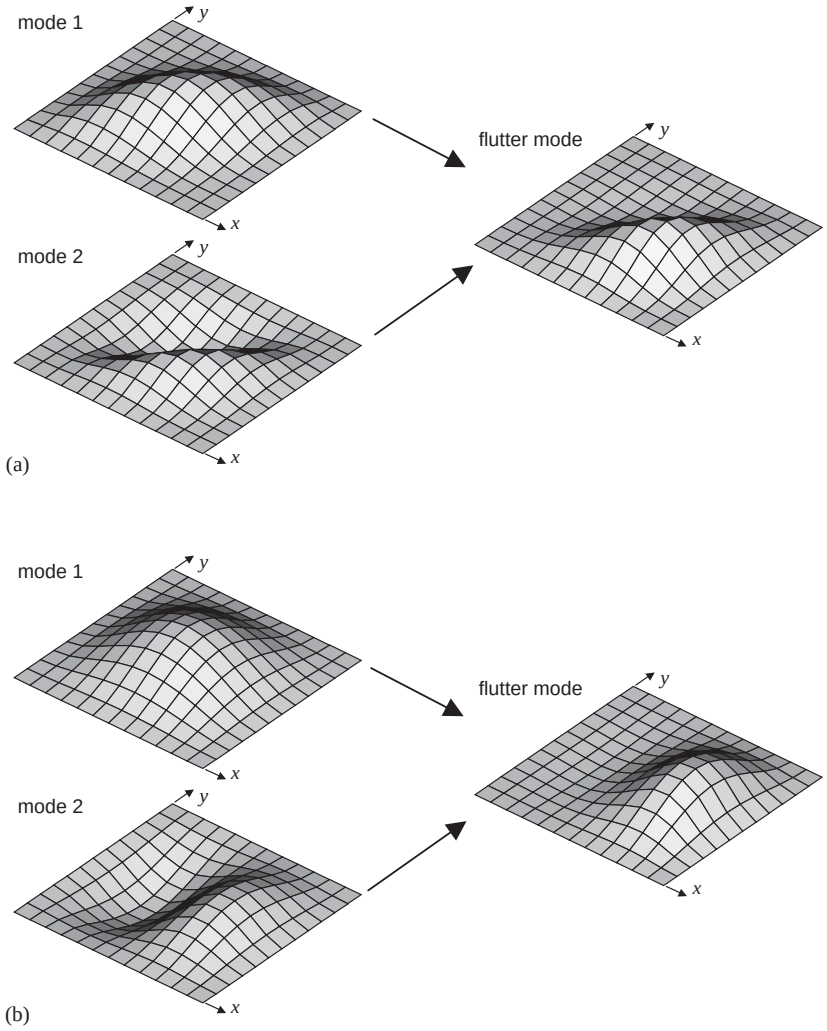


Fig. 13. Natural and flutter mode shapes of (a) $[45]_S$ plate and (b) $[90]_S$ plate.

flutter mode are shown in Fig. 10 so as to understand the relationship between $\bar{\beta}^*_{cr}$ and $\theta$. The modal loss factors of the natural modes 1 and 2 are relatively large near $\theta = 45^\circ$. The modal loss factor of the flutter mode has a value between those of the natural modes 1 and 2. This illustrates that the decrement in $\bar{\beta}^*_{cr}$ by the structural damping is large when the modal loss factors related to flutter mode is large.

The lowest critical dynamic pressures $\beta^*_{cr}$ of $[\theta]_S$ plate including structural damping are shown in Fig. 11. The values without symbols are the critical dynamic pressure of the flutter of mode 1/2 and those with symbols denote the critical dynamic pressure of the flutter of other than the mode 1/2. There are discontinuities in $\beta^*_{cr}$ at $\theta = 0,\ 25,\ 50,\ 60$, and $65^\circ$. The increment of aerodynamic damping makes the flutter mode changed at $\theta = 0,\ 50$, and $60^\circ$, too.

The mode shapes of the free vibration and flutter for $\theta = 0^\circ$ are plotted in Fig. 12. Two flutter mode shapes for $\theta = 0^\circ$. are related to mode 6. The natural and flutter mode shapes for $\theta = 45^\circ$ and $90^\circ$ are shown in Fig. 13. The flutter mode shapes show the typical frequency coalescence and have a nodal line parallel to the fiber orientation.

## 4. Conclusion

The finite element method has been applied to study the effects of distributed structural damping on the flutter boundaries of composite plates.

1. Structural damping may stabilize or destabilize the flutter instability of composite plates depending on the type of flutter. This means that the effects of structural damping are dependent on the fiber orientation of composite plates because the flutter mode can be weak or strong according to the fiber orientation.
2. Aerodynamic damping always increases critical dynamic pressure and may make the flutter mode change according to its magnitude if structural damping is included.
3. The effects of structural damping on the panel flutter of composite plates are important as aerodynamic damping decreases, i.e., altitude increases.
4. The fiber orientation of composite plates has little influence on the reduction of the critical dynamic pressure due to structural damping when aerodynamic damping is high.

## Acknowledgements

The first author acknowledges support by the University of Ulsan Research Fund of 2002.

## References

[1] P.F. Jordan, The physical nature of panel flutter, *Aero Digest* (1956) 34–38.
[2] D.N. Johns, P.C. Parks, Effect of structural damping on panel flutter, *Aircraft Engineering* 32 (1960) 304–308.
[3] E.H. Dowell, Nonlinear oscillation of a fluttering plate, *American Institute of Aeronautics and Astronautics Journal* 4 (1966) 1267–1275.
[4] J. Dugundji, Theoretical considerations of panel flutter at high supersonic Mach numbers, *American Institute of Aeronautics and Astronautics Journal* 4 (1966) 1257–1266.
[5] C.H. Ellen, Influence of structural damping on panel flutter, *American Institute of Aeronautics and Astronautics Journal* 6 (1968) 2169–2174.
[6] E.H. Dowell, Panel flutter: a review of the aeroelastic stability of plates and shells, *American Institute of Aeronautics and Astronautics Journal* 8 (1970) 386–399.
[7] C. Sander, C. Bon, M. Geradin, Finite element analysis of supersonic panel flutter, *International Journal for Numerical Methods in Engineering* 7 (1973) 379–394.
[8] R.S. Srinivasan, B.J. Babu, Free vibration and flutter of laminated quadrilateral plates, *Computers and Structures* 27 (1987) 297–304.
[9] I. Lee, M.H. Cho, Supersonic flutter analysis of clamped symmetric composite panels using shear deformable finite elements, *American Institute of Aeronautics and Astronautics Journal* 29 (1991) 782–783.

[10] V. Birman, L. Librescu, Supersonic flutter of shear deformable laminated composite flat panels, *Journal of Sound and Vibration* 139 (1990) 265–275.
[11] T.V.R Chowdary, P.K. Sinha, S. Parthan, Finite element flutter analysis of composite skew panels, *Computers and Structures* 58 (1996) 613–620.
[12] I. Lottati, The role of damping on supersonic panel flutter, *American Institute of Aeronautics and Astronautics Journal* 23 (1985) 1640–1642.
[13] G.A. Oyibo, Unified panel flutter theory with viscous damping effect, *American Institute of Aeronautics and Astronautics Journal* 21 (1983) 767–773.
[14] J.M. Whitney, *Structural Analysis of Laminated Anisotropic Plates*, Technomic Publishing Co., Lancaster, PA, 1987.
[15] D.X. Lin, R.G. Ni, R.D. Adams, Prediction and measurement of the vibration damping parameters of carbon and glass fiber-reinforced plastics plates, *Journal of Composite Materials* 18 (1984) 132–152.